
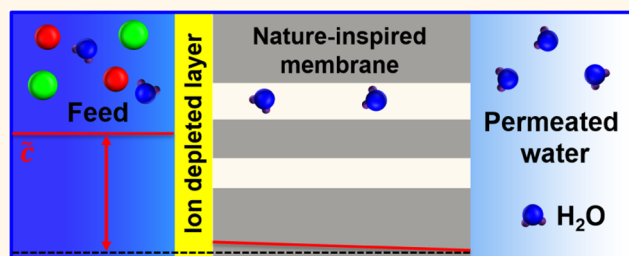




# Development of a Desalination Membrane Bioinspired by Mangrove Roots for Spontaneous Filtration of Sodium Ions

Kiwoong Kim,<sup>†</sup> Hyejeong Kim,<sup>†</sup> Jae Hong Lim,<sup>‡</sup> and Sang Joon Lee<sup>\*,†</sup> <sup>†</sup>Department of Mechanical Engineering and <sup>‡</sup>Industrial Technology Convergence Center, Pohang Accelerator Laboratory, Pohang University of Science and Technology (POSTECH), San 31, Hyoja-dong, Pohang 790-784, Republic of Korea Supporting Information

**ABSTRACT:** The shortage of available fresh water is one of the global issues presently faced by humanity. To determine a solution to this problem, the survival strategies of plants have been examined. In this study, a nature-inspired membrane with a highly charged surface is proposed as an effective membrane for the filtration of saline water. To mimic the desalination characteristics of mangrove roots, a macroporous membrane based on polyethylene terephthalate is treated with polyelectrolytes using a layer-by-layer deposition method. The fabricated membrane surface has a highly negative charged  $\zeta$ -potential value of  $-97.5 \pm 4.3$  mV, similar to that of the first layer of mangrove roots. Desalination of saline water using this membrane shows a high salt retention rate of 96.5%. The highly charged surface of the membrane may induce a relatively thick and stable ion depletion zone in front of the membrane. As a result, most co-ions are repelled from the membrane surface, and counterions are also rejected by virtue of their electroneutrality. The water permeability is found to be 7.60–7.69 L/m<sup>2</sup>·h, which is 10 times higher than that of the reverse osmosis desalination method. This nature-inspired filtration membrane exhibits steady desalination performance over 72 h of operation, successfully demonstrating the stable filtration of saline water. This nature-inspired membrane is applicable to the design of a small-scale, portable, and energy-free desalination device for use in third-world countries or small villages.



$$\tilde{c} = (\tilde{J} - (\tilde{J} \exp(Pe \tilde{x})) / \exp(Pe)) / Pe$$

(Boundary condition: inside of the membrane) ● Na<sup>+</sup> ● Cl<sup>-</sup>

**KEYWORDS:** nature-inspired, membrane, mangrove, surface  $\zeta$ -potential, desalination, polyethylene terephthalate, layer-by-layer deposition

The shortage of drinkable water has been a serious global concern for a long time.<sup>1</sup> A notable method to resolve this water shortage is the filtration of seawater, which accounts for approximately 97% of all the available water resources on Earth.<sup>2</sup> The conventional desalination method used at present is reverse osmosis (RO). However, this method has several problems, including high-energy consumption,<sup>3</sup> additional treatment of the membrane to prevent fouling,<sup>4</sup> and poor durability.<sup>5</sup> Thus, different methods for the effective desalination of seawater, such as omniphobic desalination membranes,<sup>6</sup> immobilized carbon nanotubes,<sup>7</sup> titania ceramic membranes,<sup>8</sup> and silica nanoparticle incorporated poly(vinylidene fluoride) membranes<sup>9</sup> have been introduced. These methods have high desalination efficiencies. However, most of them still have limitations that keep them from being widely adopted in industries or daily life, including a high fabrication cost, multistep fabrication requirements, and the use of harmful substances. To break this trend, we sought an environmentally friendly solution inspired by plants, as plants

have considerable adaptability in their morphology and physiology for use as survival strategies in extreme environments.<sup>10</sup>

Salinity is a major environmental stress factor affecting the growth and productivity of plants. Sodium is the principal toxic ion in saline water, which imparts osmotic and ionic stress to plants. As the salt content of a habitat increases, it becomes more difficult for plants to take in water. Plants in saline areas must effectively filter saline water to ensure their survival, as fresh water is essential for various metabolic activities. Fortunately, some plants can survive under these harsh saline conditions. These plants are called halophytes. Among halophytes, we focused on the mangrove, which is known for its special ultrafiltration system that can filter nearly 90% of

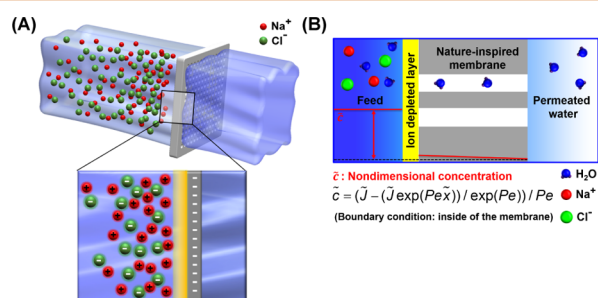
Received: October 17, 2016

Accepted: November 30, 2016

Published: December 14, 2016

sodium ions in saline water through its roots. In our previous study, the morphological, functional, and chemical properties of the mangrove roots were experimentally analyzed. The first sublayer of the outermost layer which plays a prominent role in filtering sodium ions from saline water has macroporous structures with relatively large pores of 100 nm in diameter. In addition, the surface  $\zeta$ -potential of the first layer is approximately  $-91.4 \pm 0.93$  mV, which is considerably higher than that of conventional membranes used for filtration. When the outermost layer of mangrove roots is directly used as a membrane filter, 62% of sodium ions were filtered on average.<sup>11</sup> Based on this previous study, a spontaneous water filtration method is proposed by adopting a highly negative charged membrane for utilizing the electrokinetic and hydrodynamic transportation of sodium ions of saline water.

When a substance comes in contact with an electrolyte aqueous solution, its surface acquires a surface charge.<sup>12</sup> The charged surface redistributes the nearby ions in the electrolyte solution. Ions of the opposite charge to that of the surface, known as counterions, are attracted toward the surface, whereas ions with alike charge, called co-ions, are repelled from the surface. In this study, the water filtration mechanism of mangrove roots is biomimicked to develop a desalination system. Using the electrokinetic and hydrodynamic phenomenon, a nature-inspired membrane is devised to filter sodium ions from saline water without any post-processing. Most of the sodium ions are rejected in front of the membrane, as the mangrove-inspired membrane has a highly charged surface (Figure 1A). A theoretical analysis of the concentration



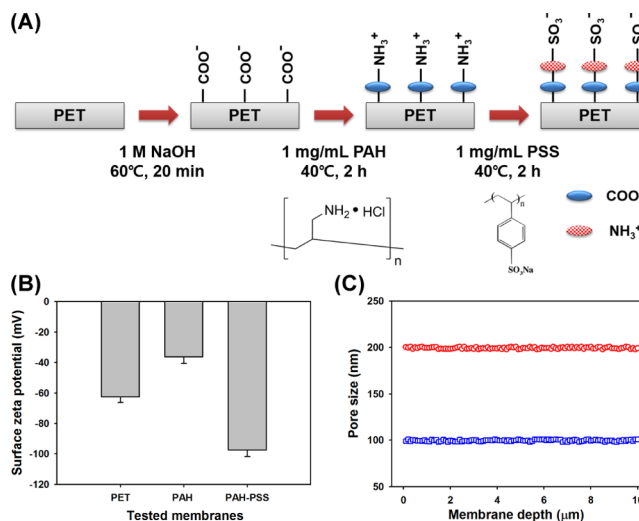
**Figure 1.** Schematic representation of the water filtration across the membrane. (A) Schematic diagram illustrating the ion rejection by the nature-inspired membrane. The left side of the membrane is filled with a sodium chloride solution. Most of the ions are rejected in front of the membrane because of the negatively charged surface. (B) Highly charged surface forms an ion-depleted layer (yellow region) in front of the membrane. Water molecules (blue) pass through the membrane, whereas sodium ions (red, small) and chloride ions (green, big) are rejected. As a result, the concentration of the feed solution is sharply decreased ( $\tilde{c}$  = nondimensional concentration,  $\tilde{j}$  = nondimensional ionic flux,  $\tilde{x}$  = nondimensional longitudinal position, and  $Pe$  = Péclet number).

variation in the membrane is conducted to demonstrate how sodium ions are filtered out by the highly negative charged membrane (Figure 1B). The fabricated membrane exhibits a high salt rejection rate of 96.5% and good water permeability of 7.65 L/m<sup>2</sup>·h during 72 h of operation.

## RESULTS AND DISCUSSION

To investigate the effects of the pore configuration and the surface charge of the proposed membrane on the filtration performance, four kinds of membranes with different pore sizes

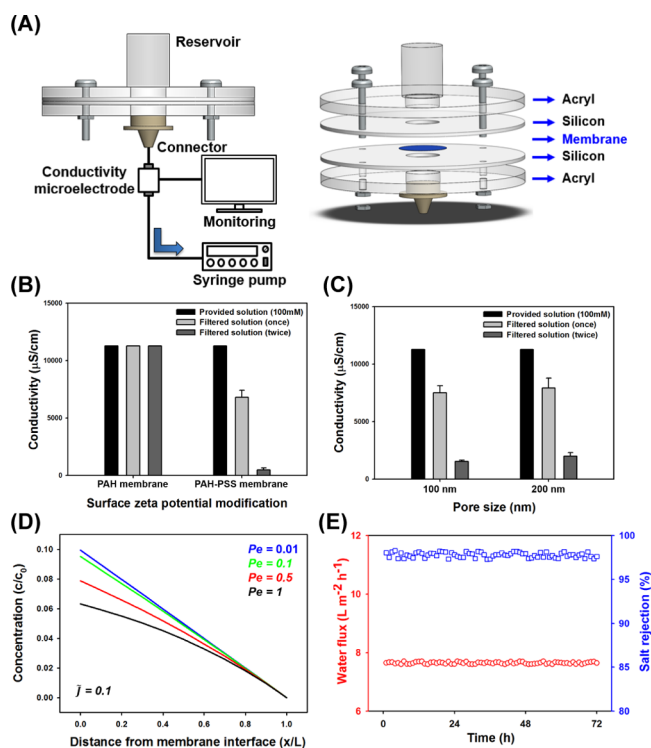
and surface  $\zeta$ -potentials were tested (Table S1). We simply assumed the electric potential gradient to be surface  $\zeta$ -potential difference along the membrane.<sup>13,14</sup> The surface  $\zeta$ -potential of the fabricated membranes was measured using a Zetasizer Nano (Malvern Co., Worcestershire, UK). Polystyrene latex beads (Malvern Co., Worcestershire, UK) with particle charge of  $-42 \pm 4.2$  mV were used as tracers (Figure 2B). The polystyrene



**Figure 2.** Membrane characteristics. (A) Illustrative schematic diagram of the sequential surface charge modification through layer-by-layer deposition of polyelectrolytes. The PET-based membrane is treated using PAH and PSS. (B) Comparison of the surface  $\zeta$ -potential of the three tested membranes. Each measurement is repeated three times. (C) Pore size variations of two different membranes with pore sizes of 100 nm (blue square) and 200 nm (red circle). They exhibit a uniform pore size distribution. The pore size distribution inside the membrane is confirmed using X-ray nano-computed tomography.

latex standard was in aqueous buffer at pH 9. The surface  $\zeta$ -potential of the carboxylation polyethylene terephthalate (PET) membrane was measured to be  $-62.5 \pm 3.8$  mV. The surface  $\zeta$ -potential of the polyallylamine hydrochloride (PAH) membrane, on which the positively charged film is deposited, was  $-36.2 \pm 4.4$  mV, and that of the PAH-PSS (polystyrene sulfonate) membrane, which has negatively charged electrolytes on the surface, was  $-97.5 \pm 4.3$  mV. The surface  $\zeta$ -potential of the PAH-PSS membrane is similar to that observed in the first layer of mangrove roots.<sup>11</sup>

Figure 3A shows the experimental setup used in the present study. A 100 mM sodium chloride (NaCl) solution was supplied into the reservoir, and filtered water exited through a connector. The connector was coupled to a conductivity microelectrode. Suction pressure was applied by a syringe pump. The suction flow rate of the syringe pump was fixed at 10  $\mu$ L/min. The syringe pump was continuously operated for 3 days to filter saline water. A silicon sheet was inserted between the membrane and acrylic plate for tight sealing. Variations in the solution conductivity according to the concentration of the sodium chloride solution are depicted in Figure S1. At the start of the infiltration process, the initial pressure applied to the test membrane was 101.31 kPa. The applied pressure was rapidly decreased to 62.53 kPa over the initial period of 45 min and then maintained at approximately 40.11 kPa (Figure S2). The provided NaCl solution was filtered through the test



**Figure 3.** Filtration of sodium ions using the nature-inspired membranes. (A) Schematic of the experimental setup. Four types of membranes with different surface  $\zeta$ -potentials and pore sizes are inserted between two silicon sheets. The feed solution (100 mM) is continuously supplied to the reservoir, and a suction pressure is applied to the bottom of the membranes. The electrical conductivity of the filtered water is monitored in real time using a conductivity microelectrode. Variations of the conductivity of the filtered water due to the modification in (B) surface  $\zeta$ -potential and (C) pore size. The filtration process is repeated twice for each case. During the experiment, the temperature and relative humidity of the chamber are maintained at  $26 \pm 1$  °C and  $52 \pm 4\%$ , respectively. (D) Variations of the nondimensional concentration inside the membrane for a fixed ionic flux of  $\tilde{j} = 0.1$ . (E) Temporal variations of the water flux (red circle) and salt rejection rate (blue square) across the PAH–PSS membrane.

membrane. This filtration process was repeated twice for each case. Each experiment for a different set of conditions was repeated three times.

The filtering performance of the membrane is illustrated in Figure 3B. When PAH membrane (case 3, Table S1) was used, the conductivities were maintained at almost the same level, even after repeated filtration. This indicates that very few sodium ions are filtered during the second filtration process. However, the conductivity of the solution filtered through the PAH–PSS membrane (case 4, Table S1) decreased from 11 270 to 6803  $\mu\text{S}/\text{cm}$  after the first filtration and then decreased from 6803 to 480  $\mu\text{S}/\text{cm}$  after the second filtration. This result indicates that the highly charged surface of the PAH–PSS membrane rejects a large amount of the sodium ions. The average concentration of the first filtered NaCl solution was 60 mM, and the average concentration of the twice-filtered solution was 3.5 mM. This indicates that approximately 96.5% of the sodium ions in saline water are filtered after repeating the filtration process. The maximum flow rate of the filtered water was approximately 20  $\mu\text{L}/\text{min}$ . In general, counterions are attracted toward the charged surface

while co-ions are repelled from the charged surface.<sup>15</sup> Thus, counterions become more dominant than co-ions in the region near the membrane surface, as the magnitude of surface  $\zeta$ -potential increases. Since the PAH–PSS membrane has a high magnitude of  $\zeta$ -potential, there is a high concentration of counterions in the near surface region and the electroneutrality is re-established at a sufficient distance away from the charged membrane surface. However, due to a Brownian motion effect, counterions are not firmly anchored on the charged surface.<sup>15</sup> As a consequence, a potential difference is established on the membrane surface, which is called the Donnan potential. The Donnan potential tends to exclude co-ions from the membrane surface. To satisfy the requirement of electroneutrality, which arises from the energetic cost of charge separation, counterions are also rejected in front of the charged surface.<sup>16</sup> The rejection of both counterions and co-ions causes the formation of an ion depletion zone on the membrane surface. As the thickness of the ion depletion zone is largely affected by the surface  $\zeta$ -potential of the membrane, the highly charged PAH–PSS membrane might form an ion depletion zone thicker than that of the moderately charged PAH membrane. As a result, the sodium ion filtered water easily passes through the PAH–PSS membrane, even though the same hydraulic pressure is applied to the PAH membrane.

To achieve a better understanding of the pore size effect on the surface-charged membrane, two kinds of membranes with pore sizes of 100 and 200 nm (case 1 & 2, Table S1) were tested (Figure 2C). The pores in the membranes had a uniform size distribution along the depth direction to minimize the electric double layer overlapping phenomenon that occurs inside the membrane. When the pore size was 100 nm, the average concentration of the first filtered water was 68 mM, and that of the twice-filtered water was 12 mM. The ion rejection rate of the carboxylation PET was slightly decreased compared to that of the PAH–PSS membrane, which has a more negatively charged surface. As the pore size increased to 200 nm, the average concentration of the first filtered water was 71 mM, and that of the twice-filtered water was 19 mM. This indicates that the membrane with the smaller pore size has a higher filtration efficiency. However, the efficiency is not significantly decreased, which implies that pore size effect does not play an important role in the scope of the present experiment when the magnitude of surface  $\zeta$ -potential is noticeably higher like the mangrove roots.

To characterize the filtration process, a theoretical analysis was conducted. For this analysis, electroneutrality, a fixed diffusivity for each ionic species, and no anion flux through the membrane were assumed. The analytic solution of the nondimensional concentration ( $\tilde{c}$ ) is given by

$$\tilde{c} = \left( \tilde{j} - \frac{\tilde{j} \exp(Pe\tilde{x})}{\exp(Pe)} \right) / Pe \quad (1)$$

where  $\tilde{j}$  is the dimensionless ionic flux through the membrane,  $Pe$  is the Péclet number, which is defined as the ratio of the convective transport rate to the diffusive transport rate,  $uL/D$  ( $u$  is the local flow velocity,  $L$  is the characteristic length, and  $D$  is the diffusion coefficient), and  $\tilde{x}$  is the dimensionless longitudinal coordinate. Detailed procedures to determine the analytical solution are appended in the Materials and Methods section. Figure 3D shows the nondimensional concentration distribution along the depth direction of the membrane depicted as a function of  $Pe$ . The condition of  $\tilde{c} = 0$  is satisfied

after filtration. The nondimensional ionic flux ( $\bar{J}$ ) is assumed to be 0.1 by reflecting the experimental conditions. The physical intuition obtained from this concentration distribution is that the condition of low  $Pe$  provides good filtration performance because it has better depletion efficiency compared to high  $Pe$  condition. One important item is that the minimum nondimensional concentration on the surface of the membrane should be less than 0.1 to guarantee the perfect filtration of saline water by using only the surface charge effect. As previously discussed, sodium ions are spatially distributed in a pattern normal to the charged surface. The theoretical analysis shows that most of the ions are rejected in front of the charged surface of the membrane by the Donnan exclusion principle because the electrostatic interaction between the charged surface and ions is dominant, while the steric effect appears to be less important.<sup>16</sup>

Water flux and the salt rejection rate through a membrane are two important factors governing the performance and effectiveness of the membrane. The water flux through a membrane was determined by measuring the volume change in the permeated water over a unit time. The water flux was maintained in the range of 7.60–7.69 L/m<sup>2</sup>·h for 3 days. The salt rejection rate of the PAH–PSS membrane was estimated by measuring the electrical conductivity of the permeated water using the equation for the salt rejection rate,  $(c - c_0)/c_0 \times 100$ . The calculated salt rejection rate was maintained at approximately 96.5% for 3 days (Figure 3E). The stable water flux and salt rejection rate indicate that fouling problems do not occur during the experiment. In addition, the effect of fouling on the changes of the membrane surface was observed using a scanning electron microscope. After the membranes were dried in a fume hood, the surface morphological characteristics of an unused PAH–PSS membrane and that of the membrane used 3 days were compared. As shown in Figure S4, the edge of the pores in the used membrane was maintained without any noticeable changes even after continuous filtration for 3 days. This implies that the PAH–PSS does not have a recognizable fouling effect on the membrane surface. This result clearly demonstrates the robustness of the proposed membrane and its potential for spontaneous filtration of saline water at very low cost. In Figure S3, the water permeability and salt rejection rate of the various membranes are compared<sup>17</sup> (MFI zeolite,<sup>18</sup> commercial polymeric seawater RO,<sup>19</sup> brackish RO,<sup>19</sup> high-flux RO,<sup>19</sup> and nanofiltration<sup>19</sup>), including the PAH–PSS membrane tested in this study. The present results are similar to those for the high-flux RO and nanofiltration cases. However, the proposed PAH–PSS membrane is easier to fabricate compared to other more conventional membranes, as the modification of the surface  $\zeta$ -potential for a membrane is relatively simple. In addition, the use of relatively larger pore sizes results in higher water permeability. Although suction pressure was applied to the membrane in this experiment, the present results would eventually be used to devise a highly efficient, portable, and energy-free desalination system.

## CONCLUSION

A spontaneous filtration membrane inspired by mangrove roots is proposed in this study. Based on the desalination characteristics of mangrove roots, highly charged membranes are fabricated using PET, PAH, and PSS. The PAH–PSS membrane has several advantages, including a simple fabrication process, high ion rejection rate, strong durability, and antifouling properties. In addition, the permeation rate of

the PAH–PSS membrane is improved by a factor of 10, compared to that of seawater RO (Figure S3). Since the fabricated PAH–PSS membrane has a relatively larger pore size, the water permeability is much higher and the hydrostatic pressure required to operate the filtration system is much less than that required for seawater RO. It is also possible to operate this filtration system without an external electric power source by applying suction pressure to the membrane with an appropriately designed reservoir structure.

When the filtering process was repeated several times, the proposed membrane would successfully desalinate the natural seawater scooped up from the seaside of Pohang (Korea) (Figure S5). The concentration of the filtered water was decreased from 312 to 3.7 mM after 10 filtration times. The water flux and salt rejection rate of the PAH–PSS membrane are fairly stable, having endured repeated testing over 3 days, irrespective of the increase in the concentration of the sodium chloride solution. Conclusively, this study demonstrates that the PAH–PSS membrane can be used as a high-performance filtration membrane for seawater desalination (Figure 1B). This membrane is suitable for use in the design of small-scale, portable, and energy-free desalination devices.

The present results are useful not only for understanding the underlying desalination mechanism of mangrove roots but also for providing the experimental data required to develop a biomimetic desalination device. The biomimetic desalination technology proposed in this study would ultimately be used for effectively resolving the serious water shortage problems facing humanity in the near future.

## MATERIALS AND METHODS

**Membrane Preparations.** To mimic the electrokinetic characteristic of mangrove roots, PET-based membranes (Sterlitech Co., Kent, USA) were treated to have a surface  $\zeta$ -potential range similar to that of mangrove root surfaces.<sup>20</sup> To increase the magnitude of surface  $\zeta$ -potential of the membrane, a layer-by-layer deposition method utilizing electrostatic forces was adopted by applying an appropriate amount of polyelectrolytes from PAH and PSS solutions (Figure 2A). The prepared PET-based membranes were rinsed with deionized water, methanol, and hexane for 2 h each and then immersed in a 1 M NaOH aqueous solution for 20 min. As a result, a carboxylation PET membrane was obtained. The carboxylate-terminated membranes were immersed in a 1 mg/mL PAH solution. This membrane is known as the PAH membrane. Thereafter, the PAH membrane was dipped in a 1 mg/mL PSS solution. It is referred to as the PAH–PSS membrane.

**X-ray Nano-CT.** The 3D morphological structures of the fabricated membranes were observed using X-ray nano-CT at the beamline using 6C Bio Medical Imaging with a Pohang Light Source-II. A 13 keV monochromatic beam was used for illumination, and the transmitted X-rays were registered by an X-ray imaging microscope (Optique Peter, Lentilly, France) located 12 mm behind the sample. The microscope had a 6  $\mu$ m thick terbium-doped Lu<sub>2</sub>SiO<sub>3</sub> (LSO:Tb) scintillator (FEE, Idar-Oberstein, Germany), a 40 $\times$  objective (UPLSAPO40X2; Olympus), and a scientific CMOS camera (Zyla; Andor, UK). The field of view was 0.41 mm  $\times$  0.35 mm, and the effective pixel size was 0.16  $\mu$ m. For CT, the sample was rotated on an air-bearing rotary stage (ABRS-150MP-M-AS, Aerotech, Inc., Pittsburgh, PA) over 180°, and its angular projections were recorded every 0.45°. CT reconstruction and quantitative analysis of the 3D images were performed using Octopus with phase retrieval support (inCT, Gent, Belgium) and Amira (FEI, Hillsboro, OR), respectively.

**Theoretical Analysis.** In general, the transport of ions along the  $x$ -axis is governed by the Nernst–Planck equation:

$$\frac{\partial c_i}{\partial t} = -\frac{\partial J_i}{\partial x} \quad (2)$$

where  $t$  is time,  $c_i$  is the concentration of the  $i$ th species,  $x$  is the longitudinal position, and  $J_i$  is the ionic flux of the  $i$ th species. The ionic flux consisting of convection, diffusion, and migration terms can be expressed as<sup>21</sup>

$$J_i = -D_i \frac{\partial c_i}{\partial x} - \frac{z_i F D_i}{RT} c_i \frac{\partial \psi}{\partial x} + c_i u \quad (3)$$

where  $D_i$  is the diffusivity of the  $i$ th species,  $R$  is the gas constant,  $T$  is the absolute temperature,  $F$  is the Faraday constant,  $\psi$  is the electric potential, and  $u$  is the flow velocity in the  $x$  direction. Combining eqs 2 and 3 leads to

$$\frac{\partial c_i}{\partial t} = \frac{\partial}{\partial x} \left\{ -D_i \frac{\partial c_i}{\partial x} - \frac{z_i F D_i}{RT} c_i \frac{\partial \psi}{\partial x} + c_i u \right\} \quad (4)$$

At steady state, eq 3 can be simplified to

$$J_+ = -D_+ \frac{\partial c_+}{\partial x} - \frac{z_+ F D_+}{RT} c_+ \frac{\partial \psi}{\partial x} + c_+ u \quad (5)$$

and

$$J_- = -D_- \frac{\partial c_-}{\partial x} - \frac{z_- F D_-}{RT} c_- \frac{\partial \psi}{\partial x} + c_- u \quad (6)$$

for 1:1 electrolyte solutions. To avoid complex analytic solutions, we assumed electroneutrality ( $c_+ = c_- = c$ ), a fixed diffusivity for each ionic species ( $D_+ = D_- = D$ ), and no anion flux through the membrane. Accordingly, eqs 5 and 6 are therefore simplified to

$$J_+ = -D \frac{dc}{dx} - \frac{FD}{RT} c \frac{d\psi}{dx} + cu \quad (7)$$

and

$$0 = -D \frac{dc}{dx} + \frac{FD}{RT} c \frac{d\psi}{dx} + cu \quad (8)$$

Combining and subtracting eqs 7 and 8 gives

$$J_+ = -2 \frac{FD}{RT} c \frac{d\psi}{dx} \quad (9)$$

and

$$J_+ = -2D \frac{dc}{dx} + 2cu \quad (10)$$

For additional simplification of the above equations, nondimensionalization is conducted by

$$\tilde{x} \equiv \frac{x}{L}, \tilde{c} \equiv \frac{c}{c_0}, \tilde{\psi} \equiv \frac{F\psi}{RT}, \tilde{J} \equiv \frac{LJ_+}{2Dc_0}, Pe \equiv \frac{uL}{D} \quad (11)$$

As a result, eqs 9 and 10 may be rewritten as

$$\tilde{J} = -\frac{d\tilde{c}}{d\tilde{x}} + \tilde{c}Pe \quad (12)$$

and

$$\tilde{J} = -\tilde{c} \frac{d\tilde{\psi}}{d\tilde{x}} \quad (13)$$

To solve these partial differential equations, proper boundary conditions are needed. By reflecting the experiment conditions of the present study, eqs 12 and 13 are solved using

$$\tilde{c} = \left( \tilde{J} - \frac{\tilde{J} \exp(Pe\tilde{x})}{\exp(Pe)} \right) / Pe \quad (14)$$

and

$$\tilde{\psi} = -Pe\tilde{x} + \ln(\exp(Pe(\tilde{x} - 1)) - 1) \quad (15)$$

with  $\tilde{c} = 0$  and  $\tilde{\psi} = 1$  at  $\tilde{x} = 1$ .

## ASSOCIATED CONTENT

### Supporting Information

The Supporting Information is available free of charge on the ACS Publications website at DOI: 10.1021/acsnano.6b07001.

Additional details about the characteristics of the test membranes, variations in the conductivity according to the concentration of the sodium solution, variations in the negative hydrostatic pressure on the test membranes, comparison of the salt rejection rates for the various membranes with respect to the water permeation rate, and variations in the concentration of the filtered natural seawater (PDF)

## AUTHOR INFORMATION

### Corresponding Author

\*E-mail: sjlee@postech.ac.kr.

### ORCID

Sang Joon Lee: 0000-0003-3286-5941

### Notes

The authors declare no competing financial interest.

## ACKNOWLEDGMENTS

This research was financially supported by the Creative Research Initiative (Diagnosis of Biofluid Flow Phenomena and Biomimic Research) of the National Research Foundation (NRF) of Korea (Contract Grant Number 2008-0061991). We thank H. Kwon and Prof. G. Lim from POSTECH in Korea for their assistance with design of filtration experiments.

## REFERENCES

- (1) Barthel, R.; Meleg, A.; Nickel, D.; Trifkovic, A. Extraction of Water for Public Drinking Water Supply. In *Regional Assessment of Global Change Impacts*; Springer: Switzerland, 2016; pp 165–170.
- (2) Zhou, D.; Zhu, L.; Fu, Y.; Zhu, M.; Xue, L. Development of Lower Cost Seawater Desalination Processes Using Nanofiltration Technologies-A review. *Desalination* **2015**, *376*, 109–116.
- (3) Zou, S.; Yuan, H.; Childress, A.; He, Z. Energy Consumption by Recirculation: A Missing Parameter When Evaluating Forward Osmosis. *Environ. Sci. Technol.* **2016**, *50*, 6827–6829.
- (4) Xie, M.; Lee, J.; Nghiem, L. D.; Elimelech, M. Role of Pressure in Organic Fouling in Forward Osmosis and Reverse Osmosis. *J. Membr. Sci.* **2015**, *493*, 748–754.
- (5) Hu, Y.; Lu, K.; Yan, F.; Shi, Y.; Yu, P.; Yu, S.; Li, S.; Gao, C. Enhancing the Performance of Aromatic Polyamide Reverse Osmosis Membrane by Surface Modification via Covalent Attachment of Polyvinyl Alcohol (PVA). *J. Membr. Sci.* **2016**, *501*, 209–219.
- (6) Lee, J.; Boo, C.; Ryu, W.-H.; Taylor, A. D.; Elimelech, M. Development of Omniphobic Desalination Membranes Using a Charged Electrospun Nanofiber Scaffold. *ACS Appl. Mater. Interfaces* **2016**, *8*, 11154–11161.
- (7) Gethard, K.; Sae-Khow, O.; Mitra, S. Water Desalination Using Carbon-Nanotube-Enhanced Membrane Distillation. *ACS Appl. Mater. Interfaces* **2011**, *3*, 110–114.
- (8) Kujawa, J.; Cerneaux, S.; Koter, S.; Kujawski, W. Highly Efficient Hydrophobic Titania Ceramic Membranes for Water Desalination. *ACS Appl. Mater. Interfaces* **2014**, *6*, 14223–14230.
- (9) Obaid, M.; Ghouri, Z. K.; Fadali, O. A.; Khalil, K. A.; Almajid, A. A.; Barakat, N. A. Amorphous SiO<sub>2</sub> NP-Incorporated Poly (vinylidene fluoride) Electrospun Nanofiber Membrane for High Flux Forward Osmosis Desalination. *ACS Appl. Mater. Interfaces* **2016**, *8*, 4561–4574.
- (10) Fujita, M.; Fujita, Y.; Noutoshi, Y.; Takahashi, F.; Narusaka, Y.; Yamaguchi-Shinozaki, K.; Shinozaki, K. Crosstalk Between Abiotic and Biotic Stress Responses: A Current View From the Points of

Convergence in the Stress Signaling Networks. *Curr. Opin. Plant Biol.* **2006**, *9*, 436–442.

(11) Kim, K.; Seo, E.; Chang, S.-K.; Park, T. J.; Lee, S. J. Novel Water Filtration of Saline Water in the Outermost Layer of Mangrove Roots. *Sci. Rep.* **2016**, *6*, 20426.

(12) Everett, D. H. *Basic Principles of Colloid Science*; The Royal Society of Chemistry: London, 2009; pp 63–75.

(13) Sung, J. H.; Chun, M.-S.; Choi, H. J. On the Behavior of Electrokinetic Streaming Potential During Protein Filtration With Fully and Partially Retentive Nanopores. *J. Colloid Interface Sci.* **2003**, *264*, 195–202.

(14) Chun, M.-S.; Lee, T. S.; Choi, N. W. Microfluidic Analysis of Electrokinetic Streaming Potential Induced by Microflows of Monovalent Electrolyte Solution. *J. Micromech. Microeng.* **2005**, *15*, 710.

(15) Masliyah, J. H.; Bhattacharjee, S. *Electrokinetic and Colloid Transport Phenomena*; John Wiley & Sons: Hoboken, NJ, 2006; pp 105–178.

(16) Fornasiero, F.; Park, H. G.; Holt, J. K.; Stadermann, M.; Grigoropoulos, C. P.; Noy, A.; Bakajin, O. Ion Exclusion by Sub-2-nm Carbon Nanotube Pores. *Proc. Natl. Acad. Sci. U. S. A.* **2008**, *105*, 17250–17255.

(17) Pendergast, M. M.; Hoek, E. M. A Review of Water Treatment Membrane Nanotechnologies. *Energy Environ. Sci.* **2011**, *4*, 1946–1971.

(18) Li, L.; Dong, J.; Nenoff, T. M.; Lee, R. Desalination by Reverse Osmosis Using MFI Zeolite Membranes. *J. Membr. Sci.* **2004**, *243*, 401–404.

(19) Guillen, G.; Hoek, E. M. Modeling the Impacts of Feed Spacer Geometry on Reverse Osmosis and Nanofiltration Processes. *Chem. Eng. J.* **2009**, *149*, 221–231.

(20) Kirby, B. J.; Hasselbrink, E. F. Zeta Potential of Microfluidic Substrates: 2. Data for Polymers. *Electrophoresis* **2004**, *25*, 203–213.

(21) Park, S.; Jung, Y.; Son, S. Y.; Cho, I.; Cho, Y.; Lee, H.; Kim, H.-Y.; Kim, S. J. Capillary Ion Concentration Polarization As Spontaneous Desalting Mechanism. *Nat. Commun.* **2016**, *7*, 11223.